Journal of Physics D: Applied Physics

PAPER • OPEN ACCESS

Dimensional scaling effects on critical current density and magnetization switching in CoFeB-based magnetic tunnel junction

To cite this article: R Phoomatna *et al* 2024 *J. Phys. D: Appl. Phys.* **57** 185002

OPEN ACCESS
IOP Publishing
Journal of Physics D: Applied Physics
J. Phys. D: Appl. Phys. **57** (2024) 185002 (8pp)
https://doi.org/10.1088/1361-6463/ad2477

Dimensional scaling effects on critical current density and magnetization switching in CoFeB-based magnetic tunnel junction

R Phoomatna[1], S Sampan-a-pai[1], A Meo[2], R W Chantrell[1,3], J Chureemart[1,3] and P Chureemart[1,3,*]

[1] Department of Physics, Mahasarakham University, Mahasarakham 44150, Thailand
[2] Department of Electrical and Information Engineering, Politecnico of Bari, Bari 70125, Italy
[3] School of Physics, Engineering and Technology, University of York, York, YO10 5DD, United Kingdom

E-mail: phanwadee.c@msu.ac.th and pc536@york.ac.uk

Received 3 October 2023, revised 10 January 2024
Accepted for publication 31 January 2024
Published 12 February 2024

Abstract

In this work, we theoretically investigate the size dependence of the magnetization reversal behavior in CoFeB-MgO-CoFeB magnetic tunnel junctions (MTJs) by employing an atomistic spin model coupled with the spin accumulation model. The former and the latter are used to construct the magnetic structure and to model the spin transport behavior, respectively. The accuracy of the approach is confirmed by investigating the dependence of the magnetic properties on the size of the MTJ. Perpendicular magnetic anisotropy (PMA) is observed for thickness less than 1.3 nm, which is in an excellent agreement with experiment. To investigate the magnetization dynamics induced by spin-polarized current, a charge current is injected into the MTJ structure perpendicular to the stack leading to a spin-transfer torque acting on the magnetization of the CoFeB layer. The results show that the critical current density to reverse the magnetization is lower for PMA-MTJ and in addition for the same injected current density the time required to switch the magnetization is shorter than for an in-plane MTJ. The results can be used as a guideline to optimize the design of high performance MTJs for STT-MRAM applications.

Keywords: magnetic tunnel junction, atomistic model, STT-MRAM

1. Introduction

The development of a spin-transfer torque (STT) magnetic random-access memory (STT-MRAM), which is a non-volatile, fast speed and low power consumption device, has been opened up by the discovery of the STT phenomenon [1, 2]. The magnetic tunnel junction (MTJ) consisting of two ferromagnets (FMs) separated by a thin insulator is a crucial component of the reading and writing processes in magnetic data storage systems [3, 4]. STT-MRAM is a novel type of non-volatile memory that utilizes magnetic characteristics and magnetization direction to store data in the form of binary bits [5]. The operation of the MTJ-based reader/writer can be controlled by injecting spin current into the structure [6–9]. The spin current interacts with the magnetization in the first FM which results in the spin-polarized current. This flows into the second FM, where the s-d exchange interaction between

* Author to whom any correspondence should be addressed.

the spin-polarized current and the local magnetization leads to switching for large values of current [10–12]. The functionality of MTJ-based devices is significantly influenced by the strength of the STT associated with the injected current density.

The optimal value of injected current density used to manipulate the direction of magnetization is an important factor for MTJ design since it is related to the performance of devices: in particular the speed and power dissipation [13]. In the reading process, the injected current density must be sufficient to detect the readback signal but not too high. Otherwise, the excessive current density can alter the direction of magnetization and causes a reading issue [14]. In contrast, for the writing process, the density of injected current should be high enough to effectively reverse the direction of magnetization. It is recommended to avoid excessively high current densities during the writing process which can result in joule heating and high power consumption. It is crucial to optimize the injected current density for both reading and writing processes. This involves determining the critical current density [15, 16], which is the minimum current density capable of switching the magnetization direction. Its magnitude is influenced by the magnetic properties of the materials and the size of the MTJ nanodot [17]. The critical current $I_{\mathrm{C}} = 2\alpha KV\frac{\gamma e}{\mu_{\mathrm{B}} g}$, where α is the magnetic damping constant, V is the volume of the system, K is the anisotropy constant, γ is the absolute value of the gyromagnetic ratio, e the electron charge and μ_{B} is the Bohr magneton. Evaluating the critical current density by considering the magnetic properties of materials and the size of the MTJ nanodot is crucial to the development of high-performance MTJs with low power consumption [18]. This, in turn, significantly contributes to the advancement of spintronic device design .

CoFeB-MgO-CoFeB MTJ has received a lot of attention as a potentially useful material for MRAM applications because it exhibits fast operating speeds, reduces power consumption, and enhances the efficiency of the device. Several experimental and theoretical studies have investigated finite size effects on the critical current density in CoFeB-based MTJ providing useful insights into the underlying physics and spin transport mechanisms governing the system [19–21]. Although the properties of the interfactial layers between layers of MTJ plays a significant role in determining device performance, it is omitted in the often-used theoretical models of MTJ to simplify calculations.

In this work, we theoretically study the size and temperature effects on the critical current density and the magnetization reversal behavior in cylindrical CoFeB/MgO/CoFeB MTJs which will be utilized to develop a high-performance MTJ structure with a size as small as 20 nm and a fast operating speed in the subnanosecond regime. The combination of atomistic and spin transport models will be employed to investigate the dynamics of the magnetization in the presence of STT. This model offers many advantages in addressing the limitations of conventional micromagnetic simulations using the Landau–Lifshitz-Gilbert–Slonczewski equation. The atomistic model not only enables the inclusion of diffuse interfaces between layers which is important for downsizing devices, but it also introduces the effects of temperature and finite size on magnetic properties. In the atomistic approach we also explicitly include the fact that the anisotropy is localized to the CoFeB/MgO interface layer. The spin accumulation model is used to investigate the spin transport behavior in the MTJ structure. The spin torque acting on the local magnetization naturally consists of adiabatic and non-adiabatic torques which are described by spin torque parameter a and b respectively. In the micromagnetic model, these spin torque parameters are assumed to be constant. However, within the spin accumulation model, the spin torque parameter a and unknown parameter b, which are time and position dependent, appear naturally and can be extracted directly. It is important to note that the parameters a and b cannot be chosen independently but reflect the phase angle between the magnetization and the spin accumulation which is determined by the (material specific) spin diffusion length. This factor is not represented by the usual micromagnetic approach. The effect of STT on the dynamics of magnetization is taken into account in the atomistic model, where the magnetization and spin accumulation are calculated self-consistently. This approach will enable the determination of the critical current density and provide insights into the behavior of magnetization reversal.

2. Methods

In this work, we use an atomistic spin model coupled with the spin accumulation model implemented in the VAMPIRE software package [22]. The atomistic model is utilized to construct the MTJ structure, taking into account the influence of diffuse interfaces and the interfacial nature of the CoFeB anisotropy. A spin accumulation model is used to investigate the spin transport behavior. The dynamical behavior of the spin accumulation and the magnetization are calculated self-consistently. The model is outlined in the following.

2.1. Atomistic model

The magnetization reversal behavior in an magnetic structure can be studied using an atomistic model via integration of the Landau–Lifshitz–Gilbert (LLG) equation to track the magnetization dynamics as follows,

$$\frac{\partial \mathbf{S}_i}{\partial t} = -\frac{\gamma}{(1+\alpha^2)}\left(\mathbf{S}_i \times \mathbf{B}_{\mathrm{eff,i}}\right) - \frac{\gamma\alpha}{(1+\alpha^2)}\left[\mathbf{S}_i \times \left(\mathbf{S}_i \times \mathbf{B}_{\mathrm{eff,i}}\right)\right] \tag{1}$$

where $\mathbf{S}_i$ is the unit vector of spin on site i, γ is the absolute value of gyromagnetic ratio, α is the damping constant of the material. The effective field ($\mathbf{B}_{\mathrm{eff},i}$) acting on spin site i can be calculated from the Heisenberg spin Hamiltonian ($\mathscr{H}$) describing the energy contributions of the magnetic system [22] given by:

$$\mathbf{B}_{\mathrm{eff},i} = -\frac{1}{\mu_s}\frac{\partial \mathscr{H}}{\partial \mathbf{S}_i}$$

with

$$\mathscr{H} = -\sum_{i<j} J_{ij}\mathbf{S}_i \cdot \mathbf{S}_j - k_{\mathrm{u}} \sum_i (\mathbf{S}_i \cdot \mathbf{e})^2 - \sum_i \mu_{\mathrm{s}}^i \mathbf{S}_i \cdot \mathbf{B}_{\mathrm{app}}$$

and $\mathbf{S}_j$ denotes the unit vector of spin on site j, J_{ij} is the nearest neighbor exchange integral between spin sites i and and j, k_{u} is the uniaxial anisotropy constant, $\mathbf{e}$ is the unit vector of easy axis and $\mathbf{B}_{\mathrm{app}}$ is the external applied field. The terms on the right-hand side (RHS) of equation (2) represent the contributions of the exchange energy, the anisotropy energy, and the Zeeman energy, respectively.

In addition to the contribution of above energies, the dipolar field is separately calculated due to the expensive computational time involved. The inclusion of the the dipolar field is determined through the implementation of a macro-cell approach [22, 23]. The system is divided into many macro-cells, where the magnetization within each cell is assumed to be uniform. The dipolar field for a macro-cell k can be expressed as:

$$\mathbf{B}_{\mathrm{dip},k} = \frac{\mu_0}{4\pi} \sum_{l \neq k} \left[\frac{3\left(\boldsymbol{\mu}_l \cdot \hat{\mathbf{r}}_{kl}\right)\hat{\mathbf{r}}_{kl} - \boldsymbol{\mu}_l}{|r_{kl}|^3} \right], \tag{2}$$

and the vector of magnetic moment in the macro-cell l containing n_{atom} spins is given by,

$$\boldsymbol{\mu}_l = \sum_{i=1}^{n_{\mathrm{atom}}} \mu_{\mathrm{s}}^i \mathbf{S}_i \,. \tag{3}$$

where μ_0 is the permeability of free space, r_{kl} and $\hat{\mathbf{r}}_{kl}$ are the distance and unit vector between macro-cell k and l. It is worth noting that the dipolar field acting all spins within the macro-cell is homogeneous. It should be noted that the dipolar field is updated infrequently due to the fact that the magnetization structure relaxes much more slowly than the timescale required for atomistic simulations.

In addition, the thermal fluctuations are taken into account in the model as a random field. The thermal field acting on spin i is determined as a random number drawn from a Gaussian distribution as follows,

$$\mathbf{B}_{\mathrm{th,i}} = \Gamma(t) \sqrt{\frac{2\alpha k_B T}{\gamma \mu_s \Delta t}}, \tag{4}$$

where $\Gamma(t)$ is obtained from a Gaussian distribution, k_B is the Boltzmann constant, T is temperature, Δt is the integration timestep and α denotes the damping constant. Consequently, the total field governing spin i including the dipolar field and thermal field is given by, $\mathbf{B}_{\mathrm{eff},i} = -\frac{1}{\mu_s{}^i} \frac{\partial \mathscr{H}}{\partial \mathbf{S}_i} + \mathbf{B}_{\mathrm{dip},i} + \mathbf{B}_{\mathrm{th,i}}$. The magnetization dynamics within the magnetic structure can be effectively modeled by integrating the total field into the LLG equation which can be numerically solved by employing the Huen scheme. This approach allows for a comprehensive understanding of the dynamic behavior in the magnetic structure.

2.2. Spin accumulation model

The MTJ can be operated by injecting charge current into the structure, which leads to the s-d exchange interaction between the spin accumulation ($\vec{\mathrm{m}}$) and local spin moment ($\mathbf{S}$), where the spin accumulation is defined as the difference of of spin up and spin down populations. This exchange interaction ($\mathscr{H}_{\mathrm{STT}} = -J_{\mathrm{sd}}\vec{m} \cdot \mathbf{S}$) subsequently results the spin torque acting on the local spin moment. The magnetization dynamic within MTJ structure in the presence of STT can be investigated via usual LLG equation. The effect of STT can be taken into account in the atomistic model as an additional field in the LLG equation as follows [22–25],

$$\mathbf{B}_{\mathrm{STT}} = -J_{\mathrm{sd}}\vec{m}. \tag{5}$$

The total effective field including the effect of spin torque is therefore,

$$\mathbf{B}_{\mathrm{eff},i} = -\frac{1}{\mu_s{}^i} \frac{\partial \mathscr{H}}{\partial \mathbf{S}_i} + \mathbf{B}_{\mathrm{dip},i} + \mathbf{B}_{\mathrm{th,i}} - J_{\mathrm{sd}}\vec{m}. \tag{6}$$

In order to observe the dynamic behavior of magnetization under the influence of STT as described above, it is necessary to substitute the spin accumulation, which acts as the source of the STT effect, into the equation of effective field in equation (6). This substitution is a requirement in the LLG equation, as indicated in equation (1). The motion of spin accumulation can be described by the expression as follows [26]:

$$\frac{\mathrm{d}\vec{m}}{\mathrm{d}t} = -\left(J_{\mathrm{sd}}/\hbar\right)\vec{m} \times \mathbf{S} - \left(J_{\mathrm{sd}}/\hbar\right)\frac{\ell_L}{\ell_\perp}\mathbf{S} \times (\vec{m} \times \mathbf{S}) - \frac{\vec{m} - \vec{m}_\infty}{\tau_{\mathrm{sf}}}.$$

where J_{sd} is the s-d exchange constant between spin accumulation and spin moment, $\hbar$ represents the reduced Planck constant, τ_{sf} is the relaxation time of spin accumulation, ℓ_L and $\ell_\perp$ are the (Larmor) spin precession length and spin coherence length, respectively. The equilibrium value of spin accumulation, denoted as $\vec{m}_\infty$, is calculated as $(n_{\mathrm{eq}}^{\uparrow} - n_{\mathrm{eq}}^{\downarrow})\mathbf{S}$, representing the difference between the populations of spin-up and spin-down states at equilibrium.

For the case that the charge current (j_e) is injected in the x direction, we replace $\frac{\mathrm{d}\vec{m}}{\mathrm{d}t} = \frac{\partial \vec{m}}{\partial t} + \frac{\partial \mathbf{j}_m}{\partial x}$ into the above equation where $\mathbf{j}_m$ is the spin current. Consequently, we obtain:

$$\frac{\partial \vec{m}}{\partial t} = -\frac{\partial \mathbf{j}_m}{\partial x} - \left(J_{\mathrm{sd}}/\hbar\right)\vec{m} \times \mathbf{S} - \left(J_{\mathrm{sd}}/\hbar\right)\frac{\ell_L}{\ell_\perp}\mathbf{S} \times (\vec{m} \times \mathbf{S}) - \frac{\vec{m} - \vec{m}_\infty}{\tau_{\mathrm{sf}}}. \tag{7}$$

Similar to the LLG equation, the precessional and damping motions of spin accumulation around the direction of spin moment can be seen in the second and third terms on the RHS of the above equation. The spin current flowing through the magnetic structure in equation (7) can be evaluated from the gradient of spin accumulation which can be expressed in the following equation,

$$\mathbf{j}_m = \beta j_e \mathbf{S} - 2D_0 \left[\frac{\partial \vec{m}}{\partial x} - \beta\beta' \mathbf{S} \left(\mathbf{S} \cdot \frac{\partial \vec{m}}{\partial x} \right) \right], \tag{8}$$

where β is the spin polarization for the conductivity, β' is the spin polarization for the diffusion constant, D_0 is the diffusion constant and x is the direction of the injected current.

Under the assumption that the spin moment reaches the steady state much more slowly than the spin accumulation, the direction of the spin moment is considered to be fixed. Therefore, the stationary solution of the spin accumulation can be solved by applying equations (7) and (8) through the use of the transfer matrix approach within a rotated coordinate system $\hat{\mathbf{b}}_1$, $\hat{\mathbf{b}}_2$ and $\hat{\mathbf{b}}_3$ which is parallel and perpendicular to the local spin moment. The solution can be decomposed into two parts: longitudinal ($\vec{m}_{\parallel}$) and transverse components ($\vec{m}_{\perp}$), taking the following form [26–29]:

$$\begin{aligned}\vec{m}_{\parallel}(x) &= \left[m_{\parallel}(\infty) + \left[m_{\parallel}(0) - m_{\parallel}(\infty)\right] e^{-x/\lambda_{sdl}}\right] \hat{\mathbf{b}}_1 \\ \vec{m}_{\perp,2}(x) &= 2e^{-k_1 x}\left[u\cos(k_2 x) - v\sin(k_2 x)\right] \hat{\mathbf{b}}_2 \\ \vec{m}_{\perp,3}(x) &= 2e^{-k_1 x}\left[u\sin(k_2 x) + v\cos(k_2 x)\right] \hat{\mathbf{b}}_3, \end{aligned} \tag{9}$$

with

$$(k_1 \pm ik_2) = \sqrt{\lambda_{\text{trans}}^{-2} \pm i\lambda_J^{-2}}$$

where $\lambda_J = \sqrt{2\hbar D_0/J_{\text{sd}}}$, the spin dephasing length $\lambda_\phi = \sqrt{2\hbar D_0 \ell_\perp/(J_{\text{sd}}\ell_L)}$, $\lambda_{sf} = \sqrt{2D_0\tau_{sf}}$ and the transverse length scale (λ_{trans}) is defined as $\lambda_{\text{trans}}^{-2} = \lambda_\phi^{-2} + \lambda_{sf}^{-2}$. Note that the unknown constant $m_{\parallel}(0)$, u and v can be calculated by satisfying the interface condition that ensures the continuity of spin current.

3. Results and discussion

3.1. Thickness dependence of the critical current density

Firstly, we consider the effect of thickness on the magnetization dynamics within the system of CoFeB(t_{CoFeB})/MgO(0.85 nm)/CoFeB(t_{CoFeB}) with cylindrical cross section, where the variable t_{CoFeB} represents the thickness as illustrated in figure 1. Specifically, we perform the analysis in two scenarios: one with longitudinal magnetic anisotropy (LMA) and the other with perpendicular magnetic anisotropy (PMA). To ensure accuracy in our simulations, the magnetic properties of CoFeB at the interface and bulk used in this work are taken from [30, 31] which consider the thickness and temperature dependence of the magnetic parameters in the CoFeB/MgO bilayer, and the results are compared with experimental data. The parameters are illustrated in table 1. The damping constant and anisotropy constant are crucial magnetic parameters for characterizing the magnetization dynamics within the CoFeB layer. These values are considered to be high at the interface region between CoFeB/MgO [30–32].

In this work, we employ an atomistic model to construct the CoFeB-MgO-CoFB system, with particular emphasis on addressing two interfaces, namely CoFeB/MgO, along with two bulk regions, as illustrated in figure 1. The system is

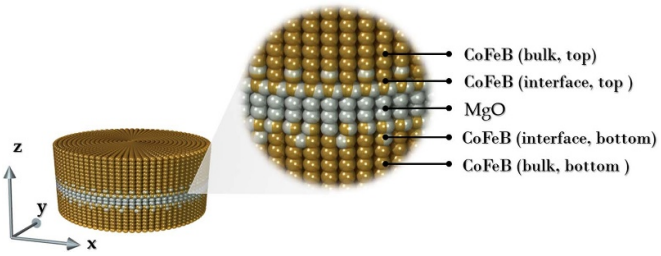

Figure 1. Schematic representation of the MTJ nanodot configuration of the CoFeB(t_{CoFeB})/MgO(0.85 nm)/CoFeB(t_{CoFeB}) system: the magnetic properties of the interfacial layer are set to be higher than those of the bulk region.

Table 1. Magnetic parameters and transport properties of the CoFeB/MgO/CoFeB system.

Parameters	CoFeB (Interface)	CoFeB (Bulk)	MgO
α	0.11	0.003	–
J_{ij} (J/link)	1.547×10^{-20}	7.735×10^{-21}	–
k_u (J/atom)	1.35×10^{-22}	0	–
μ_s (μ_B)	1.6	1.6	–
β	0.56	0.56	0.11
β'	0.72	0.72	0.14
λ_{sdl}(nm)	12	12	100
J_{sd}(eV)	0.1	0.1	0.01
m_∞(MC/m^3)	261.50	261.50	0

conceptualized as comprising five layers: CoFeB (bulk, top), CoFeB (interface, top), MgO, CoFeB (bulk, bottom), and CoFeB (interface, bottom). The influence of these interfaces is taken into account in the atomistic model through the consideration of an effective field of each spin moment in the system. The interface anisotropy and enhanced interface exchange are included explicitly in the atomistic model. Values are given in table 1. To verify the model, we examine the magnetization dynamics in the second CoFeB layer by injecting a charge current with the density of 10 MA cm^{-2} perpendicular to the plane. To investigate the influence of layer thickness on magnetization behavior, we systematically vary the thickness of the CoFeB layer, ranging from 0.9 to 3.0 nm. As demonstrated in figure 2, the out-of-plane magnetization (M_z) indicating the presence of PMA can be observed in the system with the CoFeB thickness $t_{\text{CoFeB}} \leqslant 1.3$ nm. When the CoFeB thickness exceeds 1.3 nm the magnetization of the system undergoes a transition and becomes in-plane oriented (M_x). Therefore, the critical thickness of 1.3 nm is the threshold value where the system exhibits the presence of PMA. The in-plane magnetization configuration observed in the case of a thick layer can be attributed to the dominant influence of the bulk properties, i.e. a soft magnetic material described with a magnetocrystalline anisotropy constant $K_{\text{bulk}} = 0$ J m^{-3} and the effective damping constant is 0.003, as evidenced in [31]. Thus, in the bulk the shape anisotropy of a thin cylindrical disk is the dominant anisotropy contribution. Importantly, our results demonstrate an excellent agreement with prior experimental studies

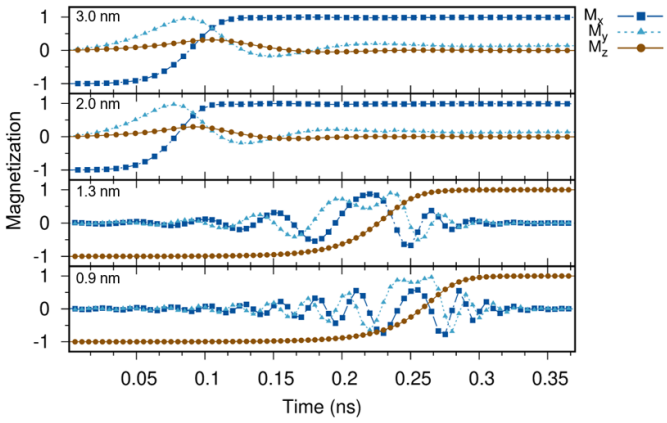

Figure 2. Magnetization dynamic in the CoFeB layer of MTJ with different thicknesses.

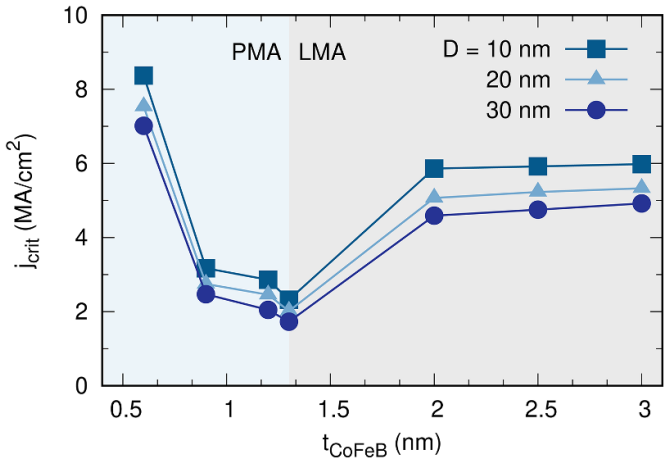

Figure 3. Relationship between CoFeB thickness and critical current density for magnetization reversal in CoFeB-MgO-CoFeB MTJ structures with different diameters.

[14, 30, 33], further validating the accuracy and reliability of our approach.

3.2. Size dependence of critical current density

In order to optimize the operating speed and minimize power consumption, it is important to examine the critical current density, which is the minimum current density required for magnetization reversal in the MTJ structure. By gaining a comprehensive understanding how to effectively control the critical current density, the design of MTJs with high performance and advanced functionality becomes achievable. For our next investigation of interest, we specifically focus on the CoFeB(1 nm)/MgO(0.85 nm)/CoFeB(0.6–1.3 nm) system with PMA and the CoFeB(2 nm)/MgO(0.85 nm)/CoFeB(2–3 nm) structure for the MTJ system with LMA. From the results shown in figure 3, it can be seen that the critical current density exhibits a minimum as a function of the CoFeB thickness. This is due to the competition between the perpendicular anisotropy at the MgO/CoFeB interface and the (in-plane) shape anisotropy of the bulk system. With increasing thickness $j_{\rm crit}$ decreases due to the reduction of the effective anisotropy of the interface layer. The minimum $j_{\rm crit}$ occurs at the thickness corresponding to the transition to in-plane magnetization. With increasing thickness the shape anisotropy overwhelms the perpendicular anisotropy leading to an asymptotic value of $j_{\rm crit}$. The critical current density is also affected by the diameter of the MTJ structure. An increase in the MTJ diameter enhances the impact of the demagnetization field, resulting in a decrease in effective anisotropy. Furthermore, larger MTJ diameters tend to exhibit an occurrence of incoherent reversal behavior [3], making magnetization reversal easier and thus reducing the critical current density as illustrated in figure 3. Our results are in good agreement with previous macrospin studies [34, 35].

Interestingly, the simulated results in figure 3 are non-monotonic, with a minimum in $j_{\rm crit}$ at a thickness of $\sim$1.3 nm. This arises from two important atomistic level factors. Specifically, the anisotropy is localised to the CoFeB layer in contact with MgO, as a result of which the net anisotropy decreases as $1/t$ the film thickness. Further, we locate the dominant anisotropy contribution to the interface, also reflecting the large spin/orbit coupling at the interface. This results in a thickness-dependent damping constant as shown by Sampan-a pai *et al* [31]. The final factor is the transition from perpendicular to in-plane anisotropy due to domination of the magnetostatic energy with increasing thickness. As a result we express the current (I_c) as follows:

$$I_c = 2\alpha K_{\rm eff} V \frac{\gamma e}{\mu_B g}, \tag{10}$$

and then we introduce the effective anisotropy, $K_{\rm eff} = |(K_{\rm bulk} - \frac{M_s^2}{2\mu_0} + \frac{K_i}{t})|$, and the system volume $(V = At)$ into the above equation. The modulus is introduced to reflect the transition to in-plane anisotropy. introducing the thickness dependence of the damping as $\alpha_{\rm eff} = 0.003 + 0.019/t$ [31] have the following expression for $j_{\rm crit}$:

$$j_{\rm crit} = \frac{2\gamma e t}{\mu_B g}\left(\left|\left(K_{\rm bulk} - \frac{M_s^2}{2\mu_0} + \frac{K_i}{t}\right)\right|(0.003 + 0.019/t)\right). \tag{11}$$

Neglecting to a first approximation the thickness dependence of α, we expect a minimum in $j_{\rm crit}$ corresponding to $K_{\rm eff} = 0$, which is around 1.3 nm, in good agreement with the numerical calculations. Our simulations depicting the size effect on the critical current density in figure 3 exhibit the same trend as previously studied in [33, 36].

Furthermore, the operating speed of MTJs, which is associated with the switching time taken for magnetization reversal, is examined. MTJs with a diameter below 20 nm are likely to be required for the future technology, therefore our investigation focuses on the influence of injected current density on the switching time in the structure CoFeB(1 nm)/MgO(0.85 nm)/CoFeB(1.3 nm) for diameters of 10, 20 and 30 nm. As demonstrated in figure 4, the switching time is highly dependent

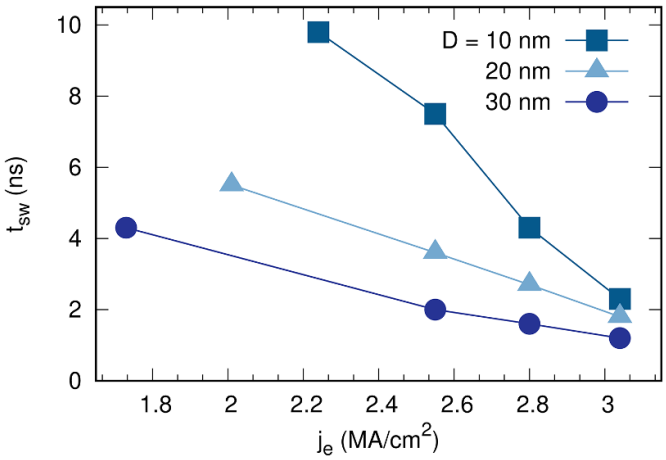

Figure 4. Magnetization switching time in the CoFeB-MgO-CoFeB MTJ with different diameters.

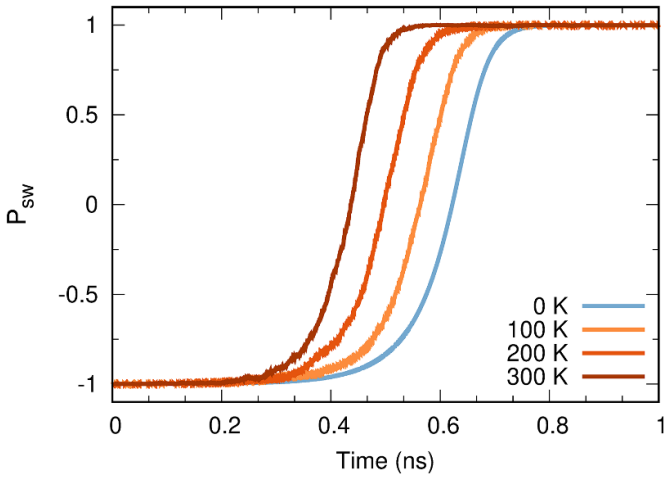

Figure 5. The time evolution of magnetization in the structure CoFeB-MgO-CoFeB MTJ with a diameter of 20 nm at different temperatures.

on both the injected current density and the diameter of the structure. An increase in injected current density gives rise to high STT, resulting in fast switching of the magnetization. Interestingly, as the diameter increases, the magnetization is more easily reversible, as evident from the critical current density and the total switching time. This is due to the reduction in effective anisotropy of the CoFeB-perpendicular MTJ caused by the increase in the contribution from the demagnetization field that results in formation of nucleation sites, which are characterized by a lower energy barrier. To achieve a switching time of less than 2 ns at 0 K, the charge current density greater than 3 MA cm^{-2} is necessary. This study emphasizes the importance of considering the system size and the interplay between interfacial and bulk anisotropy in optimizing the performance of MTJs. These factors directly impact the magnetization reversal process, which is essential for achieving desired operational characteristics.

3.3. Effect of temperature on the critical current density

To design a realistic MTJ with high operating speed in the sub-nanosecond timescale, it is important to consider the performance of devices at the operating temperature. In this work, we consider the MTJ with diameter as small as 20 nm and a switching time within the sub-nanosecond range. It should be noted that the current atomistic approach models the detail of the anisotropy, specifically its interfacial origin at the CoFeB/MgO interface and its dependence on temperature. Initially, we focus on investigating the influence of temperature on the magnetization reversal behavior in the structure CoFeB(1 nm)/MgO(0.85 nm)/ CoFeB(1.3 nm) with diameter of 20 nm. A charge current density of 4 MA cm^{-2} is injected in the MTJs. This comprehensive analysis aims to understand the intricate relationship between temperature variation and the magnetization dynamics within the MTJ system. In the presence of temperature, the magnetization switches faster as it can be observed in figure 5. The initial magnetization of the top CoFeB layer is aligned in the $-z$ direction, while the bottom CoFeB layer is oriented in the positive direction. Over time, after the current is applied to the structure, the magnetization gradually moves towards the $+z$ direction. The temperature has a significant impact on the magnetization reversal process in MTJs, particularly in terms of the time required for the magnetization to start the reversal by favoring reversal sites at the edges of the system.

As the temperature increases, the magnetization can reverse direction switching from one state to the other more rapidly than at lower temperatures, as visible in figures 5 and 6. From figure 5, it can be observed as the magnetization is reversed in less than 0.5 ns at 300 K, whereas the switching time approaches the nanosecond at 0 K. Thermal fluctuations have also a significant impact on the energy barrier, necessary to stabilize magnetization direction in the magnetic material. As a result, the magnetization becomes more susceptible to spin-polarized currents, even at low charge current density, since a lower energy barrier facilitates easier magnetization reversal. Thermal fluctuations promote incoherent magnetization reversal, where the magnetization exhibits non-uniform traits, as shown by the snapshots of the magnetization reversal at different times given in figure 5. It is worth noting that these MTJs, for diameters around 20 nm, do not exhibit a full non-coherent magnetization reversal process characterized by nucleation and propagation of a domain, as displayed in figure 6. These small non-uniformities are enough to aid the reversal without affecting significantly the thermal stability. On the other hand, the switching would involve nucleation of a reversed region that subsequently propagates across the disk for large diameters. [3, 25]. Understanding the influence of temperature on the magnetization reversal process is crucial to optimize the performance of MTJs and develop efficient spintronic devices.

Furthermore, we investigate the influence of thermal fluctuation on the critical current density in MTJs with diameter of 20 nm by varying temperature ranging from 0 to 300 K. As it results from figure 7, the critical current density is

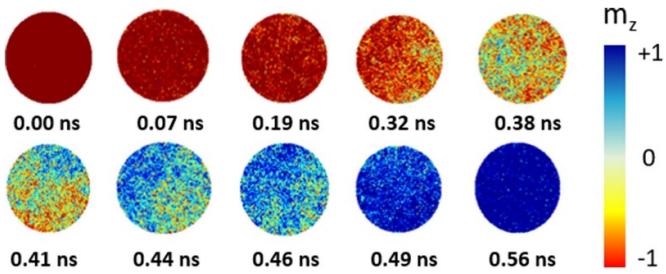

Figure 6. The visualization of magnetization dynamic in a 20 nm CoFeB-MgO-CoFeB MTJ at 300 K.

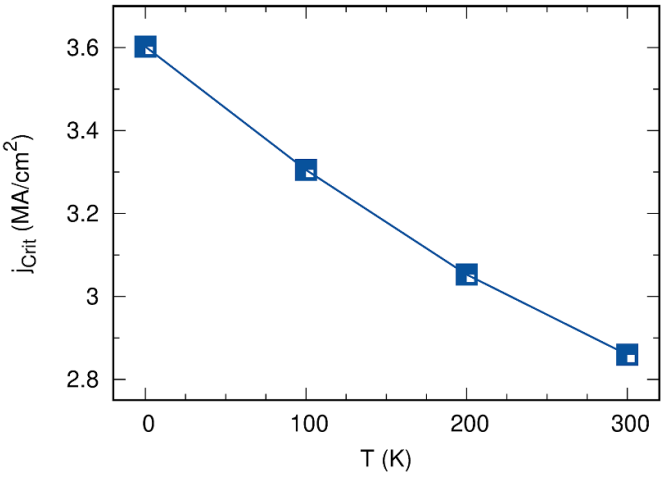

Figure 7. The critical current density of CoFeB-MgO-CoFeB MTJ as a function of temperature.

strongly affected by temperature: it decreases as the temperature increases. At a temperature of 300 K, the critical current density is found to be less than 3 MA cm^{-2}, which indicates a significant reduction of approximately 20% compared to its ideal value at zero temperature. This drop in critical current density at higher temperatures highlights the influence of thermal effects on the magnetization behavior in the MTJ structure. Thus, thermal fluctuations can provide the energy necessary to overcome the energy barrier, therefore reducing the switching time at higher temperatures. Our results are consistent with previous experimental and theoretical studies [37–40]. The insights gained from understanding the dynamic magnetization reversal behavior at different temperatures offer valuable guidance for designing and integrating next-generation data storage technologies utilizing MTJs, including advanced write head, read head, and STT-MRAM memory.

4. Conclusion

In this study, we examine the impact of size and temperature on the magnetization reversal behavior in CoFeB-based MTJs using a combination of atomistic and spin transport models. The interface between CoFeB and MgO is modeled to possess high anisotropy and damping, while the rest of the CoFeB layer is characterized by low damping and anisotropy. To achieve the MTJ with size as small as 20 nm and switching time in the sub-nanosecond timescale, it is important to consider the dimensional scaling effect and temperature effect on the critical current density which is the minimum charge current required for magnetization reversal. Our results show that the PMA-MTJ is characterized by lower critical current density and switching time compared with LMA-MTJ. We also observe the thermally assisted magnetization reversal, naturally arising from thermal fluctuations combined with finite size effects. This demonstrated a not fully-coherent switching mechanism with reversal starting at the edges of the system when temperature is considered. In addition, the temperature influences the current required for magnetization reversal. At high temperature, a smaller critical current density is required for magnetization reversal. The proposed approach allows for the design of high-performance MTJs with speeds in the subnanosecond range and sizes as small as 20 nm. The model used in this work can be a useful tool to optimize parameters to achieve the potential MTJ.

Data availability statement

The data that support the findings of this study is available from the corresponding authors upon reasonable request.

Acknowledgment

P. C. and J. C. gratefully acknowledge the financial support from Thailand Science Research and Innovation (TSRI).

ORCID iDs

J Chureemart https://orcid.org/0000-0002-1318-9266
P Chureemart https://orcid.org/0000-0002-1199-7809

References

[1] Bhatti S Sbiaa R, Hirohata A, Ohno H, Fukami S and Piramanayagam S N 2017 *Mater. Today* **20** 530
[2] Grünberg P, Bürgler D E, Dassow H, Rata A D and Schneider C M 2007 *Acta Mater.* **55** 1171
[3] Sampan-A-Pai S 2023 *Sci. Rep.* **13** 2637
[4] Tsunekawa K *et al* 2006 *IEEE Trans. Magn.* **42** 103
[5] Inci A, Isgenc M M and Marculescu D 2024 Efficient deep learning using non-volatile memory technology in GPU architectures *Embedded Machine Learning for Cyber-Physical, IoT, and Edge Computing: Hardware Architectures* ed S Pasricha and M Shafique (Springer) pp 225–52
[6] Ho M *et al* 2001 *IEEE Trans. Magn.* **37** 1691
[7] Mao S *et al* 2002 *IEEE Trans. Magn.* **38** 78
[8] Mao S *et al* 2006 *IEEE Trans. Magn.* **42** 97–102
[9] Kagami T *et al* 2006 *IEEE Trans. Magn.* **42** 93–96
[10] Zhu J-G J and Park C 2006 *Mater. Today* **9** 36–45
[11] Slonczewski J 1996 *J. Magn. Magn. Mater.* **159** L1
[12] Zimmler M A *et al* 2004 *Phys. Rev.* B **70** 184438
[13] Hayakawa J *et al* 2005 *Jpn. J. Appl. Phys.* **44** L1267
[14] Imamura H, Arai H and Matsumoto R 2022 *J. Magn. Magn. Mater.* **563** 170012
[15] Braganca P M *et al* 2005 *Appl. Phys. Lett.* **87** 112507

[16] Huai Y, Pakala M, Diao Z and Ding Y 2005 *IEEE Trans. Magn.* **41** 2621
[17] Ikeda S *et al* 2010 *Nat. Mater.* **9** 721
[18] Yoshida C *et al* 2019 *Jpn. J. Appl. Phys.* **58** SBBB05
[19] Wang Z *et al* 2016 *Nano Lett.* **16** 1530
[20] Jinnai B, Watanabe K, Fukami S and Ohno H 2020 *Appl. Phys. Lett.* **116** 160501
[21] Rao S *et al* 2021 *Electronics* **10** 2384
[22] Evans R F L *et al* 2014 *J. Phys.: Condens. Matter* **26** 103202
[23] Meo A, Chureemart J, Chantrell R W and Chureemart P 2022 *Sci. Rep.* **12** 3380
[24] Chureemart P, Evans R F L, D'Amico I and Chantrell R W 2015 *Phys. Rev.* B **92** 054434
[25] Meo A *et al* 2021 *Phys. Rev.* B **103** 054426
[26] Saenphum N, Chureemart J, Chantrell R and Chureemart P 2019 *J. Magn. Magn. Mater.* **484** 238
[27] Chureemart P, Cuadrado R, D'Amico I and Chantrell R W 2013 *Phys. Rev.* B **87** 195310
[28] Chureemart P, D'Amico I and Chantrell R W 2015 *J. Phys.: Condens. Matter* **27** 146004
[29] Saenphum N, Chureemart J, Evans R F L, Chantrell R W and Chureemart P 2021 *J. Phys. D: Appl. Phys.* **54** 395004
[30] Sato H *et al* 2018 *Phys. Rev.* B **98** 214428
[31] Sampan-a pai S *et al* 2019 *Phys. Rev. Appl.* **11** 044001
[32] Meo A *et al* 2017 *Sci. Rep.* **7** 16729
[33] Chenchen J W *et al* 2011 *Jpn. J. Appl. Phys.* **51** 013101
[34] Bouquin P, Rao S, Kar G S and Devolder T 2018 *Appl. Phys. Lett.* **113** 222408
[35] Wang H, Kang W, Zhang Y and Zhao W 2018 *IEEE Trans. Electron. Devices* **65** 5537
[36] Kang D H and Shin M 2021 *Sci. Rep.* **11** 22842
[37] Takeuchi Y *et al* 2021 *Appl. Phys. Lett.* **119** 242403
[38] Sun J Z and Safranski C 2022 *J. Magn. Magn. Mater.* **563** 169878
[39] Long J *et al* 2023 *Nanomaterials* **13** 2558
[40] Richter H J, Mihajlović G, Melendez N D, Grobis M K and Santos T S 2023 *AIP Adv.* **13** 025013